Digitalization Platform for Sustainable Battery Cell Production: Coupling of Process, Production, and Product Models

Gabriela Ventura Silva, Matthias Thomitzek, Mark Lippke, Thilo Heckmann, Hassan Karaki, Clemens Lischka, Felix Möhlen, Dominik Mayer, Jan Hagemeister, Rüdiger Daub, Jürgen Fleischer, Hermann Nirschl, Daniel Schröder, Philip Scharfer, Wilhelm Schabel, Arno Kwade, and Christoph Herrmann*

Lithium-ion batteries are used in a wide range of applications, with the electromobility sector being the main contributor to the increasing demand predicted for the next decade. Although batteries play an important role in decarbonizing the transportation sector, their production includes energy-intensive processes that hinder a more sustainable production. Moreover, the production processes are characterized by a manifold of parameters leading to complex cause–effect relations along the process chain which influences the battery cell quality. Therefore, a sustainable future for battery production and the electromobility sector depends on the environmentally and economically efficient production of high-performance batteries. Against this background, this work presents a digitalization platform based on the coupling of mechanistic models to digitally reproduce the battery cell production and provide a deeper understanding of the interdependencies on the process, production, and product levels. In addition to a description of the individual models contained in the platform, this work demonstrates their coupling on a use case to study the effects of different solids contents of the coating suspension. Besides providing a multilevel assessment of the parameter interdependencies, considering quality, environmental and economic aspects, the presented framework contributes to knowledge-based decision support and improvement of production and battery cell performance.

1. Introduction

1.1. Motivation

Lithium-ion batteries are used in multiple applications, ranging from mobile consumer devices (e.g., cellphones, laptops) to electric vehicles (EVs). The electromobility sector alone contributed 60% of the total 200 GWh worldwide demand for batteries in 2019.[1] Given the urgency to meet climate targets and provide the decarbonization of the transport sector, recent studies forecast for the European market a 10- to 15-fold growth in demand for lithium-ion batteries between the years 2020 and 2030.[2,3] A sustainable future for the production of lithium-ion batteries and the transport sector, with lower environmental impacts and high profitability, depends on environmental and economically efficient production and high-performance batteries.[4]

Battery cells are manufactured in a process chain with highly specialized and strictly interlinked processes. As a consequence, process alterations (e.g., in

G. Ventura Silva, M. Thomitzek, C. Herrmann
Institute of Machine Tools and Production Technology
Technische Universität Braunschweig (IWF)
38106 Braunschweig, Germany
E-mail: g.ventura-silva@tu-braunschweig.de

G. Ventura Silva, M. Thomitzek, M. Lippke, H. Karaki, F. Möhlen,
D. Schröder, A. Kwade, C. Herrmann
Battery LabFactory Braunschweig (BLB)
38106 Braunschweig, Germany

The ORCID identification number(s) for the author(s) of this article can be found under https://doi.org/10.1002/ente.202200801.

M. Lippke, F. Möhlen, A. Kwade
Institute for Particle Technology (iPAT)
Technische Universität Braunschweig
38104 Braunschweig, Germany

T. Heckmann, P. Scharfer, W. Schabel
Thin Film Technology (TFT)
Karlsruhe Institute of Technology
76131 Karlsruhe, Germany

H. Karaki, D. Schröder
Institute of Energy and Process Systems Engineering (InES)
Technische Universität Braunschweig
38106 Braunschweig, Germany

C. Lischka, H. Nirschl
Institute for Mechanical Process Engineering and Mechanics (MVM)
Karlsruhe Institute of Technology
76131 Karlsruhe, Germany

processing times, scrap rate) affect the entire production.[5,6] Moreover, each process is defined by various parameter interactions, leading to a manifold of cause–effect relations along the production chain which influence the battery cell performance.[7] Battery cell production is divided into three main phases (electrode production, cell assembly, and cell conditioning), whereby aspects such as cell format, material, and process technologies may vary from manufacturer to manufacturer. Electrode production usually starts with the batch-wise mixing of active materials, additives, binder, and solvent into a slurry that is coated onto a metallic substrate. The wet coating is dried and the resulting electrode is pressed between two rolls during the calendering process. Commonly, a final drying takes place before the foil is cut into single electrode sheets. The next phase, cell assembly, takes place in a dry room and is characterized by single-unit processes. For the pouch cell format, the anode, cathode, and separator are stacked and contacted before being inserted into a pouch bag. Finally, the pouch cell is filled with electrolytes and closed before being conditioned. Outside the dry room, the battery cell goes through the formation and aging processes in the last production phase.[4] The processes of drying and calendering present high power demand for a short processing time while formation presents long processing times with short power demand. These energy-intensive processes together with the dry room contribute to high energy demand in battery cell production, which not only leads to high potential environmental impacts (e.g., emissions) but also affects the economic competitiveness of the manufacturer.[8,9] Previous works have shown the influence of process parameters (e.g., duration, temperature) on the energy demand and how different configurations may contribute to a more energy-efficient battery cell production.[5,10] Process parameters also influence the electrode structure, and therefore are directly related to the cell performance at the end of production.[4,11,12] The establishment of a more sustainable battery cell production and high-performance cells depends on a deep understanding of these cause–effect relations between process, production, and product levels. Thus, there is a need for a methodology that enables a multilevel assessment of parameter interdependencies along with the battery cell production under consideration of quality as well as environmental and economic aspects to provide knowledge-based decision support and improve production and battery cell performance.

1.2. Existing Model-Based Approaches

Modeling presents a promising approach to identifying parameter interdependencies and overcoming existing challenges in battery cell production, such as improving battery cell performance and increasing energy efficiency.[5,10,11] It is also applied to digitally represent existing or planned production systems as well as

D. Mayer, J. Fleischer
Institute of Production Science (wbk)
Karlsruhe Institute of Technology
76131 Karlsruhe, Germany

J. Hagemeister, R. Daub
Institute for Machine Tools and Industrial Management (iwb)
Technical University of Munich
85748 Garching, Germany

their dynamic behavior over time by using models of the individual elements (e.g., product, processes) of a battery cell factory.[6,12,13] As a result, modeling of production systems circumvents high costs for real experiments while providing quick and quantitative results. In general, modeling approaches can be divided into mechanistic models, based on validated equations to describe a system, and data-driven models, based on mathematical algorithms to fit experimental data.[14,15]

Mechanistic models provide deeper knowledge of the cause–effect mechanisms within a system without depending on collected data, and therefore can be extrapolated to new systems.[13] Consequently, mechanistic models are better suited for reproducing products and processes across a wide range of scenarios, thus being the focus of this work. Current publications addressing the individual elements of battery cell production can be categorized into three levels of observation: process, production, and product.

Models on a process level focus on the physicochemical mechanisms and interactions between process and structural parameters within a single process. Since battery cell production is composed of highly specialized processes, there are several heterogeneous approaches tailored to best model each one of them. Starting with mixing, Lischka and colleagues deploy a discrete element method (DEM) simulation to investigate the behavior of nanoscaled carbon black (CB) aggregates for the dispersion process.[16] Lombardo and colleagues simulate the additive migration during drying using a 3D model that observes the effect of drying rate on the final electrode mesostructure.[17] Another modeling approach for the drying process is introduced by Lippke and colleagues, in which DEM is used to describe the formation of electrode structure during drying, focusing on the active material framework and the interparticle effects.[18] Sangros et al. propose a DEM approach for the calendering process to model the mechanical properties of LiNMC particles with an elastoplastic contact model as well as the mechanical behavior of the additive-binder matrix via a bond model.[19] Also for the calendering process, Meyer et al. developed a compaction model based on the Heckel equation.[20] Besides individual process models, there exist a few approaches focusing on their coupling to generate a process chain. For example, Ngandjong et al. introduce a multiscale simulation platform linking the electrode fabrication process with a coarse-grained molecular dynamics approach for electrode fabrication and a 3D continuum performance model.[21]

Besides considering processes, models on a production level also focus on material and energy flows between the production steps as well as other profitability-related indicators, e.g., machine availability. Weeber et al. present a simulation-based methodology considering machines, processes, and technical building services (TBS) to assess production throughput, machine availability, and process-specific energy demand in battery production.[5] Silva et al. present a combination of discrete event and agent-based approaches to simulate the impact of different scrap rates on energy demand and production costs.[6] This work shows that the effects on a process chain are not proportional to the alterations in scrap rate and, with that, highlights the importance of process chain simulations to dynamically analyze the interactions between machines and processes. The work by Schönemann et al. lies at the intersection of the process and production levels and proposes a multiscale simulation approach in which models for different factory levels (product units,

processes, machines, technical building services, and the building structure) are integrated, and used to support production planning.[22] While the developed framework is able to describe the process and process chain levels, the use cases displayed focus exclusively on the investigation of lead times and energy demand.

Finally, an extensive number of models on a product level with a focus on the electrochemical performance of battery cells can be found in the literature. Mechanistic battery cell models are separated into lumped-parameter equivalent circuit models, Doyle–Fuller–Newman models, and electrochemical full 3D models. The model types vary in complexity which also results in differing computation times (from a few milliseconds to hours). The Doyle–Fuller–Newman models present a good compromise regarding a sufficiently detailed abstraction of the electrochemical processes in the cell and adequate computation times. The Pseudo-2D (P2D) model is widely used and continuously extended in the literature.[10,11,23]

There are existing approaches that combine two levels: process and production or process and product. Thomitzek and colleagues present a digitalization platform consisting of a mechanistic process chain and a battery cell model to investigate the propagation of uncertain parameters along the process chain and into the final battery cell. The platform concept consists of containers for individual process models that can be coupled via the structural parameters. While the existing approaches allow in-depth insight into the cause–effect relations within the respective subsystem (i.e., process or product), battery cell production equally requires deep knowledge of the interaction of all three levels. When producing high-performance battery cells in large-scale factories, it is mandatory to understand how different performance indicators, such as quality (process chain and product level), throughput or energy demand (production level), influence each other. Against this background, this work proposes an approach to couple mechanistic
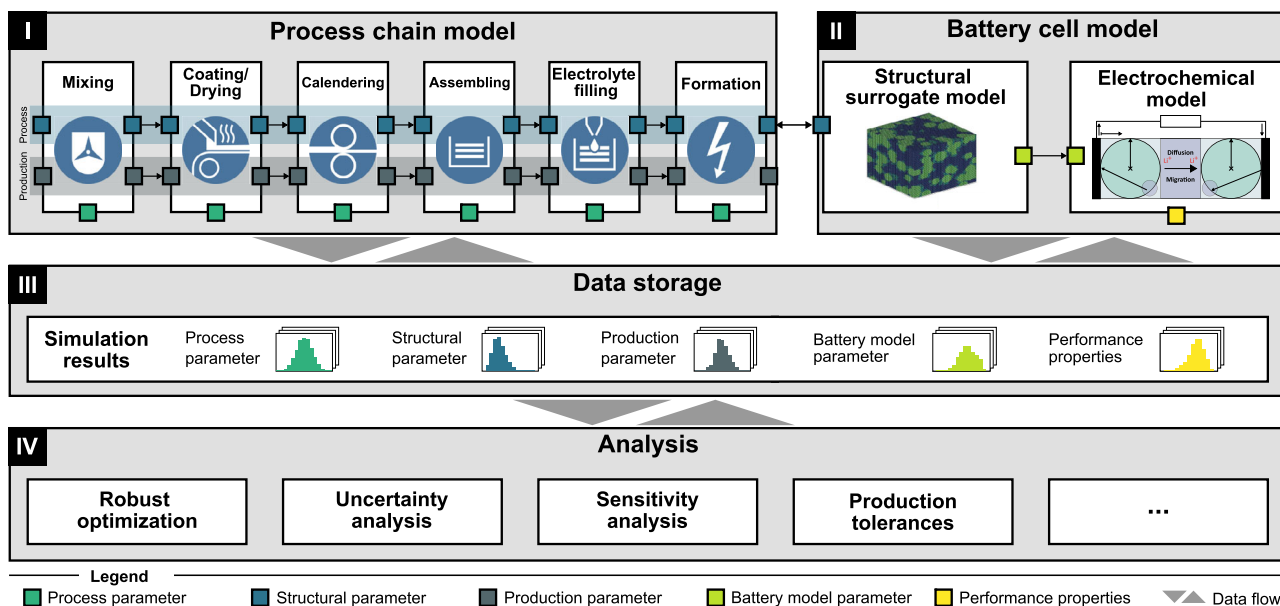
models on the process, production, and product levels by extending the digitalization platform proposed by Thomitzek and colleagues. Next to the process and product quality aspects approached in the previous version, this updated and extended framework provides a more comprehensive analysis of the cause–effect interactions between the elements within the battery cell production by also considering economic and environmental aspects, e.g., production throughput and energy demand.

The remaining article is structured as follows: Chapter 2 presents the extended version of the digitalization platform, including detailed information on the modeling approaches and parameters of each model. Chapter 3 focuses on demonstrating the coupling of models on the process, production, and product levels as well as on the application of the presented framework in a use case. Lastly, the conclusion and outlook are presented in Chapter 4.

2. Model-Based Digitalization Platform

The proposed digitalization platform is based on the coupling of mechanistic models to reproduce the battery cell production, considering cause–effect interactions and parameter interdependencies on the process, production, and product levels. The framework presented in **Figure 1** is an extension to the previously published work in ref. [13] and consists of four modules: 1) process chain model; 2) battery cell model; 3) data storage; 4) analysis.

The main characteristic of the framework is its modularity which allows the models to be used either individually or in combination. In the first module, individual process models can be coupled into a process chain model, resulting in a fully characterized battery cell as output. Building on,[13] the process chain model is extended by a production-oriented model which runs parallel to the individual mechanistic models and reproduces the material and energy flows along the process chain.

Figure 1. Framework of the modular digitalization platform to reproduce the battery cell production and assess parameter interdependencies on the process, production, and battery cell levels. Adapted under the terms of the Creative Commons CC BY license.[13] Copyright 2022, the Authors. Published by MDPI.

The characterized cell from the process chain model can be used as input to the battery cell model, which consists of the structural surrogate and electrochemical models. The input and output parameters of each simulation are stored in the data storage module, being available to be used in further models or by different analysis functions. These analyses include, for example, robust optimization[24] or identification of production tolerances.[25]

As shown in Figure 1, parameters provide the connection between models and modules. Structural parameters, which represent the characteristics of the intermediate or final products (e.g., mass loading and coating density), enable the coupling of individual mechanistic models. The electrode structure is affected by the processes and their parameter configuration which leads to a variation of the structural parameters along the process chain (e.g., porosity before and after calendering). Process parameters (e.g., line speed and temperature) connect the process and production-oriented models and, in turn, affect the material and energy flow on a production level. Lastly, structural parameters resulting from the simulated process chain provide the connection between modules 1 and 2. Similar to the real production system, each process model is defined by a manifold of parameters that interact and affect each other. By coupling the models, this complexity is expanded to the entire process chain, as shown in Figure 2, which presents the parameters considered in each model.

As shown in Figure 2, the current version of the digitalization platform is composed of eight selected processes of cathode production and cell assembly, and covers a large number of parameter interdependencies. Since models are a partial representation of a system, not all parameters of the real production system are taken into account and there are still white spots, i.e., relations not yet modeled. The wet mixing process, for example, is modeled with a population balance approach and provides the particle size distribution of the CB as output, which is not yet considered in any of the following process models. However, its coupling with the drying process is under development.

The study of the cause–effect relations along the battery cell production is based on the concept of process–structure–performance relationships: the battery cell performance is influenced by the structure of the individual electrodes, which in turn are determined by the processes along the process chain. This reproduces the interdependencies between process and product levels, allowing, for example, a deeper understanding of how different process parameters affect the battery cell performance.[11,13] Starting from the battery cell model, it also enables the definition of process parameters based on the desired battery cell performance.[24] Due to the strictly interlinked processes and the parameter interdependencies, variations in process parameters lead to impacts on the entire process chain, altering the material and energy flows. Via the coupling of the process and production-oriented models, it is possible to analyze the interactions between process and production levels, such as the effect of different process configurations on the energy demand per produced cell. Finally, the process parameters considered in the process-oriented models provide a bridge between the product and production levels and the coupling of the process-oriented, production-oriented, and battery cell models, as shown in Figure 3.

A more detailed explanation of further functionalities of the digitalization platform and its modules can be found in ref. [13].
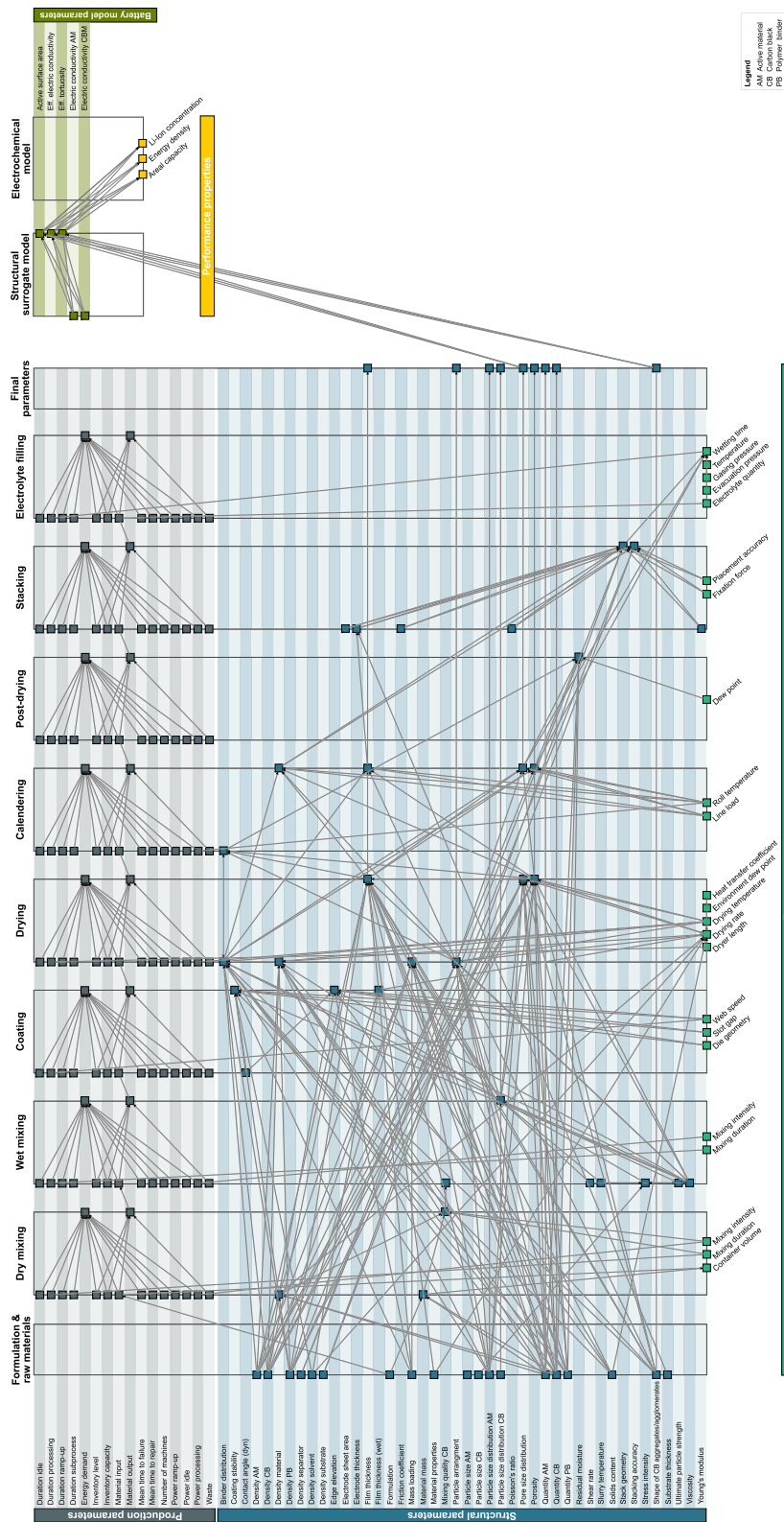
2.1. Process Chain Model

The module "process chain model" is composed of process-oriented and production-oriented models, presented in the following subsections.
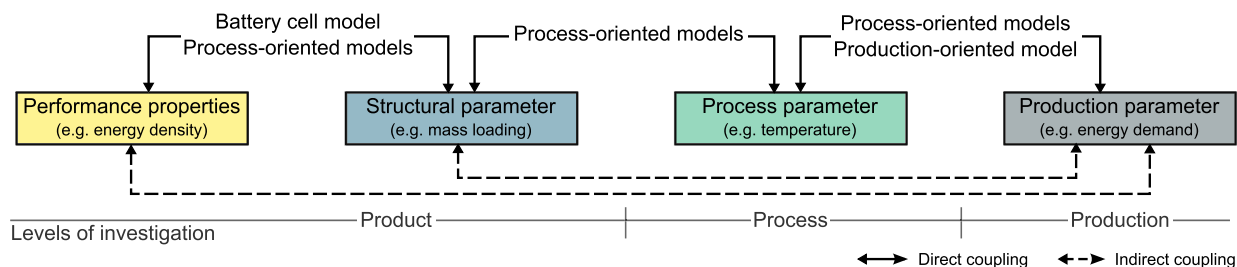
2.1.1. Process-Oriented Models

Mechanistic models focused on process and structural parameters can either be used individually or in combination in a process-oriented approach. This methodology can be applied to simulate all the processes involved in electrode production and cell assembling. The current platform version is composed of eight process-oriented models, six of which are related to cathode production (from dry mixing to post-drying) and two of which relate to battery assembly (stacking and electrolyte filling), as shown in Figure 4. Further information on the modeling approach and parameters of each individual model is described in the following.

Dry Mixing: The first process in the production of lithium-ion batteries is dry mixing, which aims to form a homogeneous mixture of the main components of the electrode materials and, if needed, de-agglomerate the CB additive. This can be achieved by different mixing devices which themselves are characterized by the energy transferred to the mixture materials. High energy mixing devices like intensive mixers (e.g., Eirich-type mixers), or annular gap mixers (e.g., Hosokawa) apply a high shear force to the materials which break the binding forces between the CB agglomerates and form smaller aggregates. The overall performance of the produced battery cells is, among other things, determined by the resulting size of the CB aggregates that are formed during mixing.[26–29]

The developed model allows us to better understand the mechanics of the dry mixing process, giving answers on how long and with which intensity the dry mixing process should be performed to form a homogeneous mixture of active material and de-agglomerated CB. Furthermore, it can then be applied for simulating up-scaled devices or different mixing devices, e.g., an intensive mixer. The model takes as input the CB content and the rotation of the high-speed stirrer. As an output, the resulting mixing behavior over time can be studied regarding its degree of mixing, de-agglomeration of the CB material defined by the resulting particle structures during mixing, and the optimal mixing parameters like intensity and mixing duration. For this, the DEM is applied to simulate the particle motion of active material particles (here spherical NMC-622 particles) and agglomerated Super C-65 CB particles. The DEM method is an established simulation technique that allows the calculation of particle movement and interaction by accounting for all acting forces and contacts of each individual particle.[30] Since the particle sizes of the modeled materials are in the range of a few micrometers,[31] a coarse-graining approach (coarse-grain factor of 100–200) is applied to increase the diameter, leading to a reduced total number of particles in the simulation and, consequently, to lower simulation times. To accurately describe the movement of

ADVANCED
SCIENCE NEWS

www.advancedsciencenews.com

Energy Technology
Generation, Conversion, Storage, Distribution

www.entechnol.de

Figure 2. Parameter matrix to consolidate the parameters and interdependencies considered in the digitalization platform. The parameter configurations used internally by the models are not represented.

Figure 3. Coupling of models and parameters that enable the analysis of interdependencies at the product, process, and production levels.
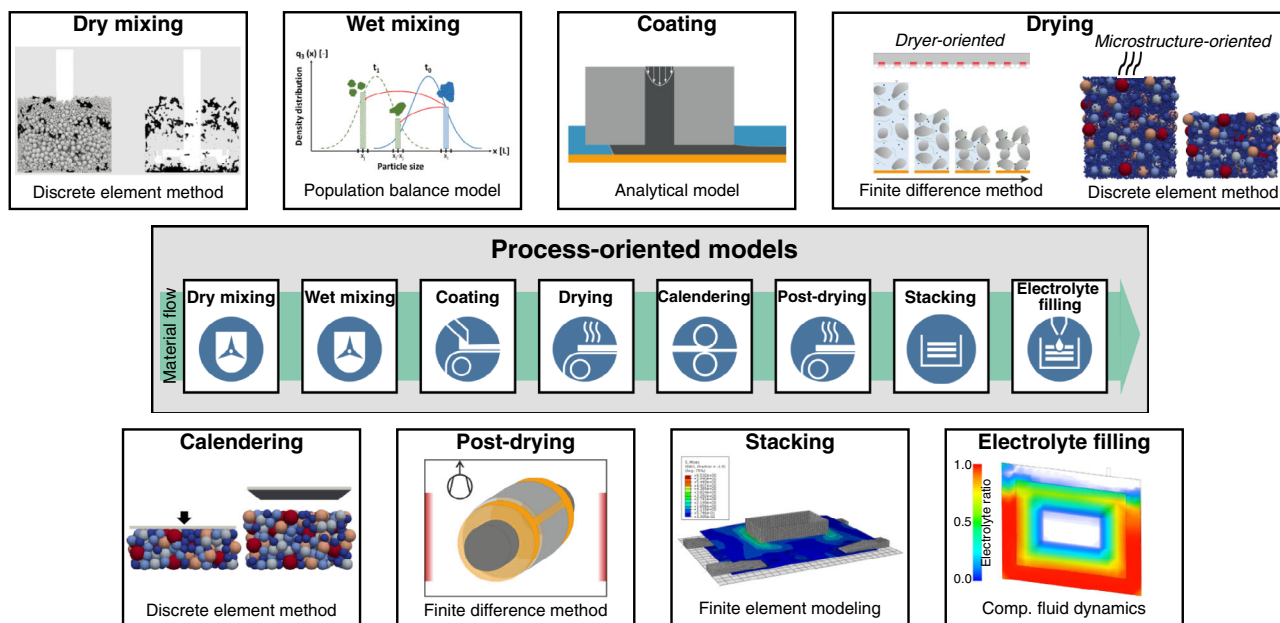
Figure 4. Overview of the processes and process-oriented modeling approaches integrated into the digitalization platform.

the coarse-grained particles, calibration measurements and simulations were performed in an RST-01 Schulze ring shear tester and a rotating drum with a diameter of 60 mm. The calibrated materials were then used to simulate the mixing and de-agglomeration behavior in a small lab scale 40 mm cup with a 30 mm high-speed stirrer (dissolver disk).

Wet Mixing: Wet mixing consists of adding solvent to the dry electrode materials and is an important step in the production of electrode slurry, as the solvent ensures wetting of the particulate components and good solubility of the binder. The formed network of the binder (e.g., polyvinylidene fluoride) with the conductive additives (e.g., conductive graphite and/or CB) and the active materials within the cathode electrode have a significant effect on the electrochemical performance. Moreover, the solid mass fraction within the slurry also influences the dispersion process as well as the coating ability and drying behavior. The distribution and size of the CB agglomerates/aggregates in the suspension determine, among other things, the electrical and ionic conductivity. Since wet mixing and its process parameters influence the size distribution of the materials used as well as the homogeneity of the slurry, it also plays a role in the mechanical and electrochemical properties of all subsequent process steps.[32–34]

The presented model is based on population balance method (PBM) to reproduce the distribution as well as temporal changes in particle size of aggregates and agglomerates particles during wet mixing. Based on the work of Finke,[35] an existing model of a Z-double-shafted kneader is adapted to a planetary mixer with a CB size distribution as input. The model output is the distribution of the CB aggregate and agglomerates at the end of the wet mixing. Using the slurry recipe and the output data, a representative generated structure of the slurry is created. Parameters such as viscosity, CB strength, or shear rate distribution of the mixer must be known in advance. The data used for calibration were obtained from.[31] The PBM is based on a discretized CB size distribution: for example, the division of an entire particle size range of about 10 μm into equal 100 nm large classes results in 100 particle size classes. Classes of 1 nm would lead to a better numerical solution, however, such an exact resolution leads to high computational efforts. In addition, the model is limited to temporal changes and takes particle size into account. Due to the assumption of a homogeneous distribution within the mixer, the explicit local resolution of the mixer device is omitted. The particle quantity in a specific particle size class changes due to inflows and outflows of the considered particle which

ADVANCED
SCIENCE NEWS

www.advancedsciencenews.com

Energy Technology
Generation, Conversion, Storage, Distribution

www.entechnol.de

reproduces the breakage of CB aggregates or agglomerates. For a successful breakage event, the fracture condition must be fulfilled, i.e., the acting force must be greater than the calculated ultimate strength of the particles, which is determined according to Raasch's model.[36] The breakage event is calibrated with a fracture probability function as well as a function of dispersion time and particle size.

Coating: The slot-die coating process is an industrial pre-metered application method for electrode processing in which the electrode slurry is applied onto the substrate (i.e., the current collector).[37–42] In this process, a slot die guides the liquid slurry through two lips onto the substrate and establishes menisci that generate a uniform coating across the entire coating width. The flow of the liquid slurry is pre-metered and determines the film thickness in the cross-web direction in addition to the web speed.[43] Coating defects that occur outside the process window set the limitations for achievable film thicknesses at given process parameters. Possible defects are swelling, air entrainment, and low-flow streaks. Swelling occurs if the pressure inside the coating bead is high enough to push the liquid out of the gap between the slot die and substrate in the counter web direction. Low-flow streaks and air entrainment occur if the pressure inside the coating bead is low enough for air to break the menisci and leave voids in the coating.[44]

A process window predicts the appearance of coating defects based on an analytical solution of the pressure balance in the coating gap for given process parameters (e.g., web speed and pumping speed).[43–47] Schmitt et al. extended the process window to highly viscous and particle-loaded Li-ion battery coatings.[38] This process window is integrated into the simulation platform as a quality gate, to assure physically meaningful process conditions. The input parameters for the process window are the solids content, mass loading, density of the solids and solvent, coating speed, viscosity of the dispersion, and surface tension of the solvent. The output of the model is the information on whether the particular parameter set yields a stable coating. Furthermore, the expected coating defects (e.g., low-flow limit) can be identified.

Drying—Dryer-Oriented: The dryer-oriented model replicates the interaction between the dryer and the wet electrode film subsequent to the coating process. The drying of porous goods traverses through various phases until it is considered dry. The first phase poses the shrinkage of the wet film due to solvent evaporation, the consolidation of the porous structure, with a more or less constant drying rate.[48–50] The second phase starts as soon as the porous structure affects the kinetic of the solvent evaporation. Eventually, during the third drying stage, residual solvent desorbs from the structure.[51] Hereby, the system parameters of the dryer influence the drying speed of an electrode as well as the physical properties of the solvent and the film. Kumberg et al. explained, modeled, and validated this complex interaction for graphite-based anodes with a water-soluble binder system.[52,53] This model is adapted to the material system of N-methyl-2-pyrrolidone (NMP)-based cathode by implementing respective material properties. The physical properties of the solvent NMP along with the thermal material properties of the solids assure the adequate representation of the cathode slurry in the drying model. The heat transfer coefficient and the temperature of each dryer segment in the multi-stage dryer represent the influence of the dryer on the drying process. The dryer considered in this study is a three-stage convective dryer with a length of $3 \times 2\,m$. The model is based on a mass and enthalpy balance of the drying electrode film, discretized over the time by finite differences. The output of the model is the time-resolved drying rate that considers individual dryer segments as well as multiple mass transport resistances that change as the film drying propagates.

Drying—Microstructure-Oriented: The second drying model focuses on the formation of the active material structure using a DEM simulation.[54] The active material particles are explicitly modeled according to their particle size distribution, while the CB particles are combined into monodisperse CB agglomerate particles to reduce the computational effort. In addition, different dispersion and dry mixing processes can be mapped by setting a higher CB porosity,[26,55] which manifests itself in a changed number of CB agglomerate particles or by coating CB onto the active material particles. In the future, it is aspired to determine this information directly from the dispersion model. First, the particles are randomly placed along the wet film height according to their fractions in the formulation. The wet film thickness depends on the solvent content of the suspension, desired areal loading, and formulation used. The interparticle interactions are mapped using Van der Waals interactions.[56] All fluid effects in the suspension are imposed on the particles by appropriate surrogate models. These include hydrostatic buoyancy force, fluid friction forces, lubrication force,[57] and capillary force of the fluid level.[58] This avoids the need for a computationally expensive coupling with a computational fluid dynamics (CFD) simulation. The fluid surface decreases with a constant sinking rate,[59] which is derived from the dryer-oriented model. At the end of the simulation, the particles form a self-supporting particle framework. Based on the particle alignment, the coating thickness and porosity can be determined. Furthermore, the resulting exact particle structure may be handed over to the calendering simulation.

Calendering: The structure development of the electrode during the calendering process is modeled using the calendering model of Sangros and colleagues based on DEM.[19,60] The active material is represented explicitly, while the inactive material is represented by solid bridges. These solid-state bridges are capable of transmitting not only forces but also torques. The mechanical properties of these solid-state bridges (e.g., stiffness, strength, and damping) are determined by means of a calibration process via the overall mechanical behavior of an electrode during calendering since these are not directly accessible experimentally and are also subject to many model assumptions.[19]

The active material structure from the drying simulation (microstructure-oriented) is used as the starting structure. The electrode is compacted by means of a vertically sinking plate until the desired calendering stress is reached. The calendering gap achieved is compared with the experimentally achieved gap size and will be used as a calibration or validation criterion. Vice versa, the simulation can also be gap-controlled. Subsequently, the direction of movement of the plate is reversed and the electrode undergoes elastic recovery. Analogous to the drying simulation, structural parameters such as layer thickness and porosity can be derived from the resulting structure.

Post-Drying: The vacuum post-drying process provides the final moisture removal prior to cell assembly[61,62] and is important as the amount of moisture inside a cell affects the lifetime and performance of a battery.[61–63] This batch process takes place in an oven that facilitates a low relative humidity by heating the drying good and periodically flushing the chamber with dry inert gas.[62] During post-drying, moisture desorbs from the individual components of a cell and is removed from the dryer's environment. The sorption behavior of battery components depends on the component as well as the process steps faced by the electrodes.[51,62–66] Furthermore, some battery components express a hysteresis in the sorption behavior with water.[51,65] These circumstances demand a well-adjusted and -designed post-drying process.[62] A low relative humidity inside the dryer triggers this desorption of the water. After the post-drying process, the cell components are exposed to dry-room conditions (controlled dew-point and temperature). Due to the increase in relative humidity compared to the post-dryer, the components resorb water to a certain extent. The amount of resorbed water is lower compared to the initial water content prior to post-drying due to the hysteresis in sorption behavior.

A model based on the finite difference method (FDM) is developed to investigate the water content inside an electrode over time inside the post-dryer. The FDM discretizes a simulation domain into a mesh and solves equations along it considering differences between mesh points. For the post-drying simulation, the water mass balance is discretized over the electrode width and time and solved numerically with a partial differential equation (PDE) solver. The input parameters are the initial water content, system parameters of the dryer (e.g., temperature and pressure), and structural parameters of the electrodes (e.g.porosity and tortuosity). The outputs of the simulation are the time-resolved water content inside the electrode and the moisture content after drying.

Stacking: In stacking, a precise overlap of the anode and cathode is an important factor in ensuring optimum ion exchange. Especially in Z-folding with single sheets or single sheet stacking, accuracy is a significant quality parameter to be ensured in the stacking process. In addition, the homogeneous density of the stack is an important aspect of the subsequent filling of the cell. FEM is suitable for simulating the stacking process and the mentioned parameters, since the behavior of the entire electrode in interaction with the adjacent machine elements is of interest.

The FEM model presented in this work reproduces the single sheet stacking and is divided into two sub-simulation models. First, the alignment and pickup of the tolerance-impaired electrode sheet are simulated, whereby the electrode geometry has a significant influence on the accuracy of the pickup.[67] For that, the main input parameters are the geometry of the electrode such as length, width, and corrugation, the initial position of the electrode as well as material data such as Young's modulus or friction coefficients. The result of the simulation is the relative position of the electrode sheet to the gripper. In the second simulation model, the actual stacking takes place. For this purpose, the result of the first simulation, i.e., the gripper with a gripped electrode, is imported into the second model. The electrode is then placed with the gripper on the stack and the electrode and the existing stack are fixed with the blank holders. This process is iterated for the anode, cathode, and separator, so that a stack is built. The limiting factor is the computing time. The stack accuracy is determined by the relative position of the corner nodes of the mesh at the cathode or anode after finishing the simulation. Further, the stack geometry can be extracted to assess the homogeneity of the stack.

Electrolyte Filling: Once the cells have been stacked, contacted, and packaged, a liquid electrolyte is introduced into the cell during the filling process, which enables the transfer of lithium ions within the battery cell. The process consists of dosing (i.e., filling the void volume surrounding the cell stack) and subsequent wetting (i.e., absorption of the liquid into the pores of the cell components). The process duration and cell performance are significantly influenced by the process parameters[68] and cell properties.[69] Dosing and wetting are of great importance for the industrial production of battery cells since their process times generate a significant cost point.[70] Additionally, the filling process is located at the end of the production chain where most of the value has already been created, increasing the impact of production errors.
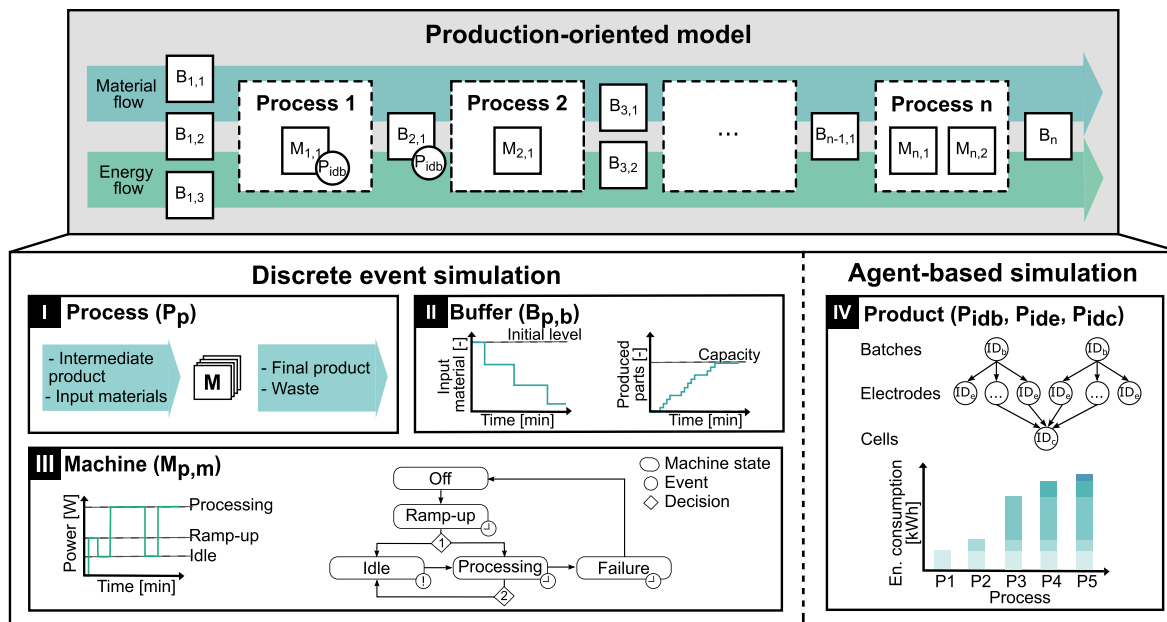
One approach to model the filling process is using CFD, i.e., a numerical analysis of liquid and gaseous fluid flow. While the process duration of the dosing takes a few seconds to minutes, the wetting takes a few hours, which is a challenge for the modeling due to the different time and size scales. To overcome this challenge, the dosing and wetting are split into two partial models. For the wetting simulation, a small 3D section of an NMC cathode with a width of 25.15 µm is used to study the flow of electrolytes through and into the porous electrode microstructure. The structural parameters such as the overall porosity, pore size distribution, and particle arrangements can be varied based on the structures simulated in previous production steps such as calendering. As a result, data such as pressure drop, electrolyte mass flow, and permeability of the porous region are exported from the wetting simulations and applied in the simulations of the dosing. To do this, the geometry of the cell housing and the cell stack are imported and process parameters such as the electrolyte temperature, dosing pressure, and gassing pressure are defined in the simulation environment. Via the interaction of the dosing and wetting simulations, the effect of varying electrode properties on the electrolyte filling process times can be studied without costly experimental studies.

2.1.2. Production-Oriented Model

The production-oriented model runs parallel to the process-oriented models presented in Figure 4. Based on production parameters (e.g., power demand and material input) and selected process parameters (e.g., web speed and temperature), this model reproduces the material and energy flows between processes within the electrode and battery cell production, as shown in **Figure 5**.

The model combines discrete event and agent-based modeling approaches and consists of four generic entities: 1) process; 2) buffer; 3) machine; 4) product. The first three entities are defined by the user during the simulation initialization and are personalized by defining the production and process parameters. The product entity, on the other hand, is generated during

2200801 (8 of 16)

ADVANCED
SCIENCE NEWS
www.advancedsciencenews.com

Energy Technology
Generation, Conversion, Storage, Distribution
www.entechnol.de

Figure 5. Modeling approaches and entities of the production-oriented model to reproduce the material and energy flows in the battery cell production.

the simulation and passed from one process to the other along the process chain. The development based on generic entities provides an easy adaptation of the process chain, facilitating the addition of new machines or integration of alternative processes.

In the discrete event simulation, changes in the entities (e.g., processes, machines, and buffers) are triggered by events (e.g., presence of input material or machine failure) at discrete points over time.[71] This approach reproduces the interaction and dependencies between entities, the material and energy flows as well as the complexities of real production systems. As shown in Figure 5, three entities are considered in the discrete event model: 1) process; 2) buffer; 3) machine. At the simulation start, the number of machines at each process as well as the inputs (e.g., intermediate product, input materials) and outputs (e.g., final product, waste) are defined. Each process has at least one machine and one buffer for input material. A buffer can either store input or output resources. In the case of input resources, the buffer level is defined at the simulation start. For output resources, the buffer maximum capacity is defined. Machines can also act as buffers and temporally store finished materials. Lastly, each machine entity may present five states: off, ramp-up, idle, processing, and failure. At the beginning of the simulation, every machine is turned off and goes into ramp-up when input material is available. The idle state can be further divided into idle due to starvation (i.e., the machine is waiting for input material) or blockage (i.e., the processing is over, however, the final material can be neither stored in the buffer or handed over to the next machine). The state changes are triggered by timely defined events (e.g., process time is over) or events related to material availability. Moreover, average power demand is assigned to each machine state which generates a machine electrical load profile, as demonstrated in Figure 5. The focus of the agent-based approach is on representing the product entity

(i.e., intermediate and final products). For that, an identification code is assigned to each product (e.g., batch, electrode, and battery cell) and product-specific information during processing (e.g., material quantity and energy demand) is stored. The dependencies between the product entities are also considered: many electrodes are produced from one batch, and one battery cell is composed of various electrodes. Furthermore, the product entity enables the coupling of the two modeling approaches in the production-oriented model, since a product is either in a buffer or in a machine. In addition, changes in the product location trigger, for example, changes in the machine states.[6]

The simulation results comprehend key performance indicators related to the production, such as throughput, machine utilization as well as material and energy demand from product to process chain level. Additional information on the changes in the machine state and process duration over time is also provided. These results enable a better understanding of dependencies between processes in addition to information on material and energy efficiency. Previous works based on the production-based model assessed the production bottlenecks with a focus on an energetic perspective[72] and the effect of different scrap rates on the process chain.[6]

2.2. Battery Cell Model

The battery cell model, the second module of the presented framework (Figure 1) is used to evaluate the electrochemical performance of the digitally manufactured electrode. It consists of two submodels: the structural–surrogate model and the electrochemical model. The former consists of surrogate polynomials for a 3D structure model, which was introduced by Laue and colleagues.[73,74] It receives input parameters for the composition and structure of the electrode, e.g., volume fractions of each active material and conductive-binder-matrix, porosity, and the

limits of the particle size distribution. Subsequently, the model generates 3D voxel-based microstructures following a stochastic distribution of particle sizes. The generated microstructure is afterward converted into a resistance network and the effective electrical conductivity and effective tortuosity are determined. Furthermore, the active surface area is computed by counting all the voxel faces which are not in contact with any other faces. In comparison to the commonly implemented Bruggeman approach,[75] this model takes into account the composition of the solid phase and the spatial distribution of particles. Thus, it can deliver a more accurate representation of the relationship between the electrode structure and its effective transport properties.

The output of the structural–surrogate model, i.e., the active surface area a_s, the effective tortuosity τ_{eff}, and the effective electrical conductivity of the solid phase $k_{s,eff}$, as well as further electrode structural parameters (i.e., porosity and thickness) serve as inputs for the electrochemical model. This model is a Doyle–Fuller–Newman-type cathode half-cell pseudo-2D model, parameterized using experimental discharge curves, as described by Thomitzek and colleagues.[13] With the electrochemical model, discharge simulations can be carried out to determine the achievable capacity based on the given structural parameters, from which then the volumetric energy density can be calculated. Furthermore, the model allows the investigation of concentration profiles during discharge, which contributes to a deeper understanding of the physiochemical interactions taking place.

3. Use Case

The digitalization platform is used to reproduce the battery cell production in a parameter study considering three solids contents (50, 60, and 70%) for the cathode formulation. Existing works have demonstrated the effects of increased solids content, such as alterations in the electrode structure and electrochemical performance as well as reduction in drying time and energy demand.[4,33,76,77] Different from these works with a focus on individual effects, this use case analyzes and quantifies a variety of aspects. For that, the battery cell model, production-oriented model, and three selected processes of the process-oriented models (coating, drying, and calendering) are considered. **Figure 6** presents the models, process chain as well the structural and process parameters considered in the use case. Due to white spots, i.e., interdependencies between processes that are not yet modeled, as discussed in Chapter 2, the processes of wet mixing, stacking and electrolyte filling are not considered in this use case.

The structural and process parameters used in the process-oriented and battery cell models correspond to the reference cathode of the ProZell competence cluster, also shown by Thomitzek and colleagues in the previous application of the digitalization platform.[13] For all three scenarios, material-intrinsic parameters (e.g., particle density), demanded mass loading (14.3 mg cm^{-2}), and demanded coating density (3.01 g cm^{-3}) remain constant. For the production-oriented model, the considered production (e.g., power demand) and process (e.g., duration) parameters were gathered in the pilot line of the Battery LabFactory Braunschweig during the production of pouch cells with 10 compartments, as presented in ref. [7].

3.1. Process Chain Model

3.1.1. Process-Oriented

Coating: Within the digitalization platform, the coating model considers the coating thickness of the wet film as a function of the coating width, web speed, and suspension volume flow as well as the physical boundaries (e.g., air entrainment) regarding the coating step for the electrode production. The simulated coating window predicts film stability during the application of the cathode slurry onto the current collector (substrate) via slot-die coating, as presented in **Figure 7** for the 50% solids content. The results of the coating window for the three scenarios and respective solids contents are listed in **Table 1**.
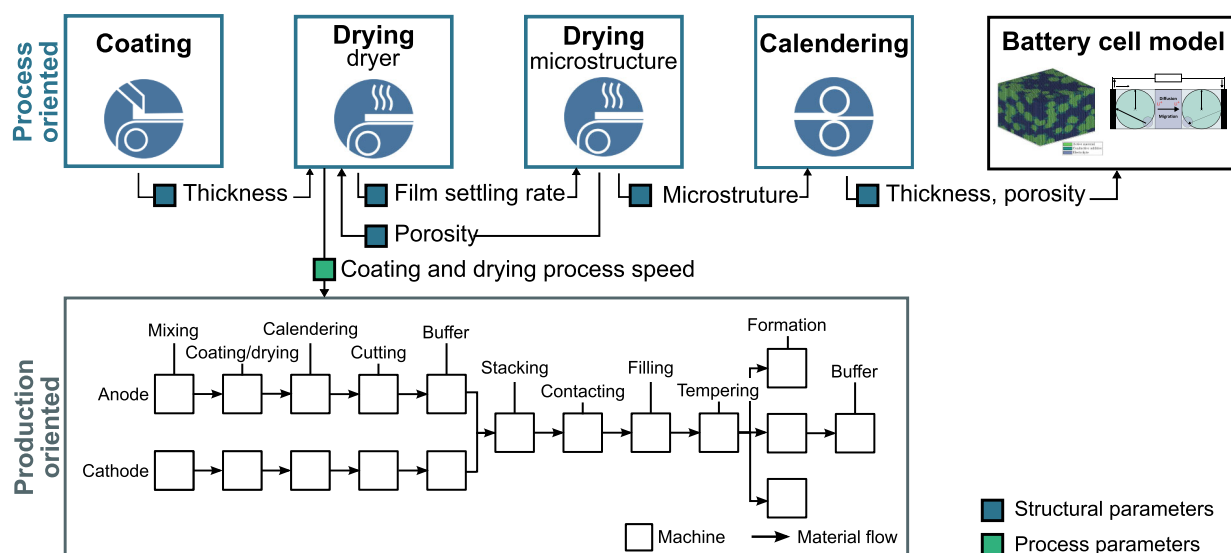
Figure 6. Overview of the models and parameters considered in the use case.
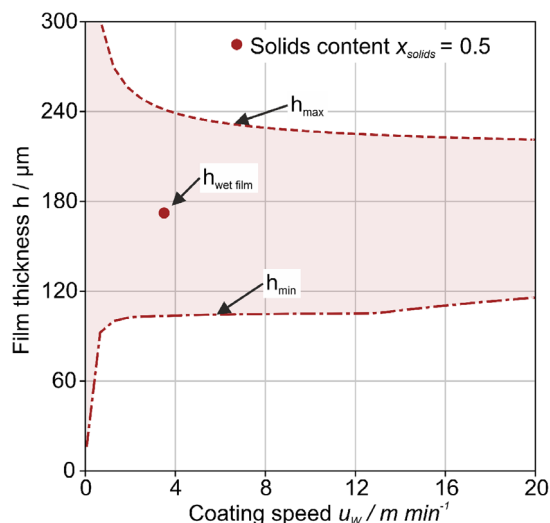
Figure 7. Coating window for the slot-die coating of the 50% solids content cathode.

Table 1. Wet film properties of the simulated cathodes after slot-die coating.

Solids content [%]	$h_{wetfilm}$ [µm]	h_{min} [µm]	h_{max} [µm]
50	173	104	242
60	127	79	160
70	93	88	113

As shown in Table 1, the wet-film coating thickness changes as the solids content varies to achieve a constant dry mass loading. The increase in particle content caused by higher solids contents increases the viscosity as well, narrowing the process-parameter window in which a stable coating can be established. The difference between the minimal stable wet-film height (h_{min}) and the maximal stable wet-film height (h_{max}) also decreases for higher solids contents. The change of the solids content and, therefore, solvent content affects the viscosity which, in turn, influences the coatings stability window of the cathode slurry. A higher viscosity fluid leads to higher pressure in the coating system, making the process susceptible to coating defects. Thus, the process parameters need to be adjusted more precisely compared to lower solids contents. Lastly, the coating thickness of the wet film is transferred from the coating process to the drying simulation as a structural parameter.

Drying: The stable, defect-free wet film obtained from the slot-die coating is passed to the drying model. The dryer is a three-zone convective dryer with an adjustable heat transfer coefficient and temperature in each zone and a total length of 6 m. The simulation of the drying step is subdivided into dryer-oriented and microstructure-oriented models. The FDM model focuses on the interaction between the dryer and the drying electrode as the DEM elucidates the microstructure formation. Both models complement each other to provide a holistic description of the drying process, as shown in Figure 6. The results of the dryer simulations are listed in **Table 2**.

Table 2. Structural information of the simulated cathodes after the complementary drying simulations. Thickness and porosity represent the values after the drying process.

Solids content [%]	Web speed [m min^{-1}]	Thickness [µm]	Porosity [−]
50	3.5	61.68	0.46
60	5.0	60.38	0.45
70	7.0	58.47	0.43

Initially, the interaction between the dryer and the wet electrode is considered. The settings regarding heat transfer coefficient and temperatures at each zone (80, 100, 120 °C) of the dryer remain constant throughout the case study and the web speed is maximized to optimize the spatial efficiency of the dryer. An increase in the solvent content while maintaining the mass loading of the dry electrode results in an increased amount of solvent that needs to be removed during the drying step. Consequently, the achievable web speed decreases as more solvent needs to be removed during the drying step. Economically, this variation in drying speed affects the overall capability of the production line and reduces the electrode yield per time. Detailed information on the effects of different web speed rates on the production level is discussed in the Subsection Production-oriented.

The variation of solvent content also affects the drying profiles in the dryer segments. The film settling rate over time is an output parameter that is required by the subsequent DEM drying model. Additionally, a time-resolved evaporating rate is an output of the simulation. This evaporation rate provides further information about the mechanism inside the electrode film while drying and could be coupled with additional simulation models, e.g., for binder diffusion.

In the DEM drying model, the influence of the solvent content is taken into account in two ways. On the one hand, higher solvent content rates lead to an increase in wet film thickness. On the other hand, a higher solvent content is expected to result in a lower suspension viscosity and thus a less intensive dispersion process. According to Bockholt et al.,[32] a lower dispersion intensity results in a lower porosity of the CB binder network of the dried electrode. This effect is represented in the DEM simulation by a lower porosity of the CB. For a solids content of 70 wt%, a CB porosity of 75% was calibrated from preliminary experimental work by means of calibration simulations. Since no experimental data were available for the calibration of the lower solid fractions, CB porosities of 77.5% and 80% were assumed to demonstrate the basic functionality of the setup. It was found that higher CB porosities result in higher coating thicknesses, as shown in Table 2. A CB porosity of 70% results in a coating thickness of 58.1 µm. For CB porosities of 77.5% and 80%, coating thicknesses of 60.0 and 61.29 µm were achieved, respectively. The film settling rate was determined by repeated iteration with the dryer-oriented drying simulation: the dryer-oriented model requires structural parameters such as porosity, which are determined by the microstructure-oriented simulation. The microstructure-oriented simulation, however, requires the film settling rate of the dryer-oriented simulation.

Calendering: The structures generated in the drying step are transferred to the calendering simulation. First, all CB

agglomerates are removed and solid bridges are formed, according to the representation of the inactive material presented in the model of Sangros et al.[60] The volume fraction of the solid bridges corresponds to the volume fraction of the inactive material in the solid mixture. Mechanical bond parameters stiffness and damping were kept constant, since the influence of the different solids contents and the induced dispersion intensity on the mechanical properties of the CB-binder-matrix was not known. Calibration of the mechanical bond parameters was performed using the data set of Diener et al.[78]

The goal of the calendering process was to achieve an electrode density of 3 g cm^{-3}. For that, the coating thickness was varied at the point of maximum compaction (corresponding approximately to the calender gap minus the substrate thickness). The layer densities, porosities and thicknesses achieved and the gap size required for this purpose are shown in **Table 3**.

Table 3 presents slight variations in gap size and, consequently, in the minimum thickness during calendering. Since the influence of the solvent content on the mechanical properties of the inactive material matrix was not taken into account, a discussion of these slight variations is not appropriate.

Lastly, the electrode structures obtained with the calendering simulation can be transferred to the CFD simulation of the electrolyte filling as an Stl-file. However, this coupling is out of the scope of this use case. The coating thicknesses and porosities determined based on these structures are transferred to the electrochemical simulation.

3.1.2. Production-Oriented

The production-oriented model is applied to assess the effects of different solids contents on the production level by considering the alterations in the material and energy flows. From a material perspective, the solvent quantity needed in the wet mixing process is lower for higher solids contents. As described in Table 2, lowering the solvent contents allows increasing the web speed in the coating and drying processes to 3.5, 5.0, and 7.0 m min^{-1}. The web speed at the calendering process is also adjusted for the three scenarios since the processes in the electrode production are strictly interlinked. From an energetic perspective, the average power demand (W) of the machines is mainly affected by the process temperature and not by the different solids contents and web speeds. As discussed by Thiede and colleagues,[79] web speed does not belong to the parameters with the highest influence on the power demand in the drying process. Since the process temperatures during drying and calendering are constant for the three scenarios, the average power demand

also remains constant. However, due to higher web speeds, the process duration is reduced, leading to changes in the energy demand (Wh) per batch.

Cathode and anode are manufactured in separate production lines which converge in the battery cell assembly line, as reproduced in Figure 6. Formation is the only process with more than one machine. Buffers for finished materials are added at the end of electrode production (capacity of ten batches) and cell finishing (unlimited capacity). The process chain capacity as well as the process and production parameters considered in the simulation derive from data gathered in the BLB pilot line. The simulation period covers 1 year of around-the-clock production. For all three scenarios, no scrap rate and a machine availability of 95% during processing are considered. Since the individual process-models focus on cathode production, the parameters for the anode processes remain constant. The aspects related to the material and energy flows resulting from the production-oriented model are summarized in **Table 4**.

As shown in Table 4, the throughput of the electrode and cell production increases for higher solids content and web speed. Although the higher web speeds lead to shorter production times in the cathode production, the amount of produced anode and cathode batches remained almost the same in every scenario, since electrode production is limited by its buffer capacity as well as by processes of the cell production (e.g., tempering and formation). Furthermore, the presented throughput growth causes an increase in the average machine utilization rate (i.e., share in processing state). The average rate from mixing to formation grows by 1% and 9% when the solids contents are increased from 50 to 60% and from 50 to 70%, respectively.

From an environmental perspective, increasing the solids content and web speed leads to a reduction in the total and specific energy demand. Between the scenarios with 50% and 60% solids content, the total energy demand was reduced by 3%. From 50% to 70% solids content, the total energetic reduction represents 9%. These values are based not only on the energy demand associated with processing but also on idle states. The calculation of the specific energy demand considered every produced part, including the ones stored in intermediate buffers at the end of the simulation. The values for specific energy demand presented in Table 4 vary from known values for pilot lines.[8] This difference can be explained by the high energy demand

Table 3. Structural information of the simulated cathodes after calendering. Porosity represents the value after the calendering process. Gap size represents the value during compression deducting the thickness of the current collector.

Solids content [%]	Thickness [μm]	Density [g cm^{-3}]	Porosity [−]	Gap size [μm]
50	47.55	3.01	0.302	27.4
60	47.58	3.01	0.302	26.3
70	47.42	3.02	0.300	29.0

Table 4. Throughput and energy demand for the three simulated scenarios with increasing solids contents and web speeds. The quantity of produced electrodes stored in the buffers is also considered in the calculation of specific energy values.

		50% − 3.5 [m min^{-1}]	60% − 5.0 [m min^{-1}]	70% − 7.0 [m min^{-1}]
Throughput	Anode [batch]	185.00	187.00	198.00
	Cathode [batch]	185.00	187.00	197.00
	Cell [tsd. cells]	10.74	10.89	11.57
Energy demand	Total (excl. dry room) [MWh]	202.24	199.12	197.94
	Specific [Wh Wh^{-1}]	799.97	776.64	728.29
	Specific [Wh cell^{-1}]	17.20	16.70	15.66

associated with nonproductive machine states. Limitations in the production capacity, typical of a pilot line, combined with low utilization rates lead to a large share of the total energy demand caused by idle times due to starvation and blockage.

Finally, a closer look at the process level shows the coating and drying process as the main contributor to the presented reduction in the energy demand. Moreover, considering the share of machine states at each process, the idle times of the electrode and cell production are mostly caused by the limiting buffer capacity (i.e., blockage).

3.2. Battery Cell Model

The battery cell model receives as input values the porosity and layer thickness passed by the calender model as well as information about the formulation and the simulated structure of the cathode. Discharge simulations are subsequently carried out to determine the achievable capacity and energy density. As

Table 5. Mean and standard deviation used to produce the normal distributions of porosity and coating thickness for the uncertainty analysis.

| Structural parameter	Mean	Standard deviation
Coating thickness [μm]	47.516	0.950
Porosity [−]	0.303	0.006

mentioned in the calendering results, the cathodes were processed to a density around $3.0\,g\,cm^{-3}$ for all three solids content. Consequently, the porosity and coating thickness are almost identical for every scenario, as can be seen in **Table 5**.

Thus, a comparison of the discharge properties of the three points would yield similar results. For this reason, an analysis of the C-rate dependency was carried out instead, using the average porosity and the thickness from the three scenarios. The results of this analysis are presented in **Figure 8**.

In Figure 8a, three discharge curves are presented, which were simulated at three different C-rates (C/2, 1C, and 2C) to represent different types of applications. It can be seen from this graph, that increasing the discharge current density leads to a lower achievable areal capacity due to the increased transport resistances at higher C-rates. To analyze the robustness of the achievable volumetric discharge energy density against uncertainties in its structural parameters, an uncertainty analysis was carried out. Herein, a normal distribution was generated for the porosity and coating thickness using a standard deviation of 2%, as shown in Table 5, and a sample size of 2,000. These distributions were then passed to the battery cell model to compute the energy densities, in a similar fashion to Schmidt and colleagues.[11] It was assumed that the ratio between the amounts of active material and the conductive-binder-matrix remained constant. The result of the uncertainty analysis shown in Figure 8b shows that the width of energy density distribution increases with increasing C-rate. This implies that the
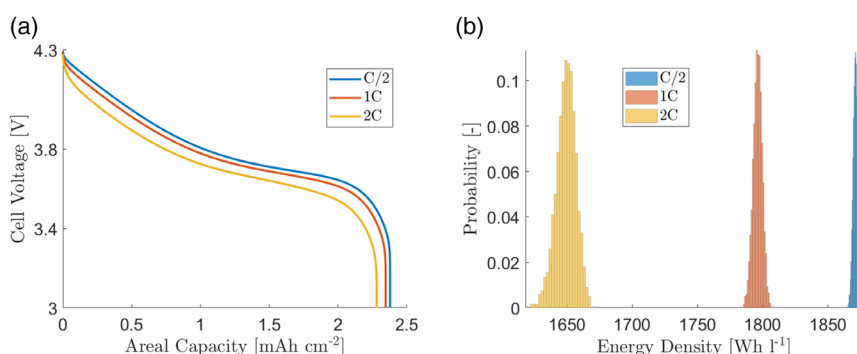
Figure 8. Results of case study with the battery cell model: a) discharge curves and b) uncertainty analyses at different C-rates.
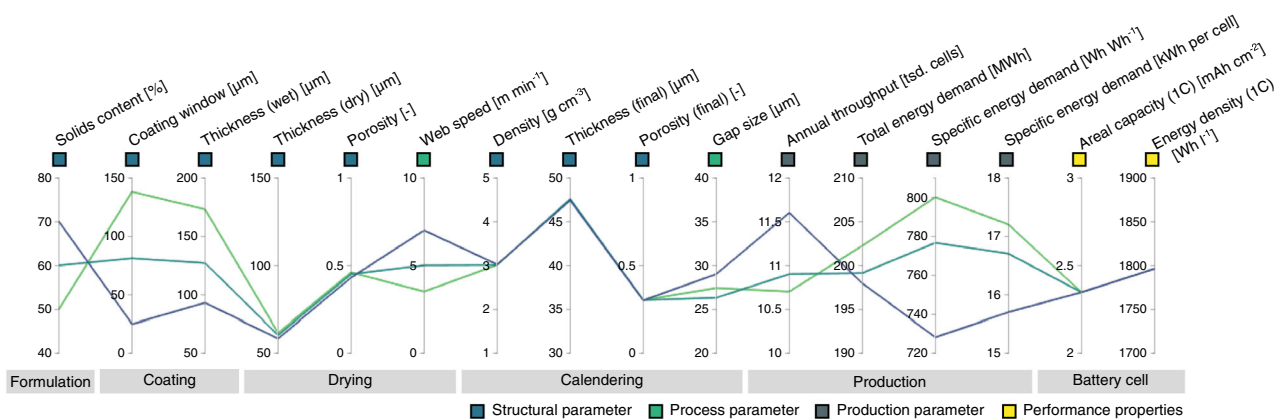
Figure 9. Consolidation of the use case results on the process, production, and product levels.

sensitivity of the energy density against uncertainties in the porosity and the coating thickness increases for higher discharge current densities.

Figure 9 consolidates the use case results and presents how structural, process, and production parameters as well as performance properties are affected by the three solids contents (50%, 60%, and 70%).

The results show that process, production, and product levels are not equally influenced by a variation in the solids content. While some parameters (e.g., coating windows and thickness (wet)) present a strong variation towards increasing solids content, others parameters (e.g., thickness (dry) and porosity) present smaller variations. In other cases (e.g., final property and energy density), the results remain constant for the three scenarios. Therefore, Figure 9 demonstrates the importance of multilevel analysis to deeply understand the cause–effect relations along the process chain.

4. Conclusion and Outlook

This work presented a digitalization platform to support the environmentally sustainable production of battery cell production with low battery cells under consideration of quality, environmental and economic aspects. For that, the framework proposed by Thomitzek and colleagues,[13] composed of process-oriented and battery cell models, was extended to a production level with a model focused on reproducing material and energy flows. The coupling of mechanistic models on the product, process, and production levels took place via the exchange of structural and process parameters. Thereby, the platform allowed a digital reproduction of the battery cell production and a comprehensive analysis of the parameter interdependencies along the process chain.

The individual models and their modeling approaches were described, followed by a matrix that consolidated the parameters of each model and highlighted their interdependencies. The current platform version allows to investigate a large number of cause–effects mechanisms between the parameters of six processes of cathode production and two processes of cell finishing. Since the models are a partial representation of the considered systems, there are relations not yet modeled that will be considered in the next platform versions.

As a demonstration of the multilevel coupling of the models, the framework was applied to a use case to identify and quantify the impact of three different cathode solids contents (50, 60, and 70%) on battery cell production. This application comprehended the coupling of four process-oriented models (i.e., coating, dryer-oriented and microstructure-oriented drying, and calendering) as well as the production-oriented and battery cell models. For each formulation, the process-oriented models simulated the effects on the electrode structure (e.g., porosity, coating thickness, density) and process parameters (e.g., web speed). The analysis on the process level allowed to investigate the electrode quality and the cause–effect relation between processes. The three web speed values were then passed to the production-oriented simulation which provided an analysis of the environmental and economic aspects, including throughput and energy demand. The analysis on the production level enabled not only to study the influences on the processes directly affected by the varying web speeds, but

also to understand how these changes affect the entire process chain. Furthermore, results such as idle times and machine utilization contributed to the identification of limiting elements of the production. Finally, the structural parameters resulting from the process-oriented models were passed to the battery cell model in which the effects on the performance properties were simulated. Since the final coating thickness and porosity for all three solids contents were similar, the model resulted in similar battery performance properties (e.g., areal capacity and energy density). In addition, discharge curves and uncertainty analyses for three C-rates rates were simulated. The results showed that the sensitivity of the energy density against uncertainties in the porosity and the coating thickness increases for higher discharge current densities.

In general, the results showed different trends toward an increase in the solids contents at each level of investigation. Although the structural parameters (e.g., thickness, porosity) for the coating and drying processes as well as the window for the coating stability presented variations, the final parameters related to the electrode structure were similar for all three scenarios due to the constant density in the calendering process. Consequently, the battery cell model resulted in similar performance properties, however, the uncertainty analysis indicated how sensitive battery performance is to variations in electrode structure for different applications. Lastly, the results on the production level presented a reduction of energy demand for increased throughput and lower machine utilization rates. The complexity of the results highlights the importance of multilevel analysis to deeply understand the mechanisms behind the parameter variations. The proposed digitalization platform represents, therefore, a valuable tool for comprehensive decision-making under consideration of multiple evaluation criteria and their cause–effect relations. This is critical for planning and improving battery cell production, as it helps to increase battery cell performance and support more environmentally sustainable and economical production.

The presented methodology can be applied to investigate alternative process technologies and battery materials. Future works will focus on the further development of the digitalization platform and the integration of new processes and parameter interdependencies. For that, other aspects such as the microstructure after calendering will be closely investigated. Further activities also focus on the validation of the entire process chain and battery cell models. Furthermore, further analysis will investigate adaptations to process parameters and production configurations to increase the battery cell performance, production profitability, and energy efficiency.

Conflict of Interest

The authors declare no conflict of interest.

Data Availability Statement

Research data are not shared.

[1] VDMA Battery Production, *Roadmap Battery Production Equipment 2030: Update 2020*, VDMA Battery Production, Frankfurt, Germany **2020**.

[2] V. Beermann, F. Vorholt, *Europaische Bateriezellproduktion Expandiert: Marktanalyse Q4*, (Ed.: VDI/VDE Innovation + Technik GmbH), VDI/VDE Innovation + Technik GmbH, Berlin, Germany **2021**.

[3] International Enegy Agency, *Global EV Outlook 2020: Entering the Decade of Electric Vehicle?*, IEA International Energy Agengy, France **2020**.

[4] A. Kwade, W. Haselrieder, R. Leithoff, A. Modlinger, F. Dietrich, K. Droeder, *Nat. Energy* **2018**, *3*, 290.

[5] M. Weeber, J. Wanner, P. Schlegel, K. P. Birke, A. Sauer, *Procedia Manuf.* **2020**, *43*, 32.

[6] G. V. Silva, M. Thomitzek, T. Abraham, C. Herrmann, in *Simulation in Produktion und Logistik*, Vol. AM 177, Cuvillier Verlag, Göttingen, Germany **2021**, pp. 227–236.

[7] A. Turetskyy, S. Thiede, M. Thomitzek, N. von Drachenfels, T. Pape, C. Herrmann, *Energy Technol.* **2020**, *8*, 1900136.

[8] M. Thomitzek, N. von Drachenfels, F. Cerdas, C. Herrmann, S. Thiede, *Procedia CIRP* **2019**, *80*, 126.

[9] acatech, *Roadmap Integrierte Zell- und Batterieproduktion Deutschland*, Gemeinsame Geschäftsstelle Elektromobilität der Bundesregierung (GGEMO), Berlin, Germany **2020**

[10] M. Thomitzek, O. Schmidt, F. Roder, U. Krewer, C. Herrmann, S. Thiede, *Procedia CIRP* **2018**, *72*, 346.

[11] O. Schmidt, M. Thomitzek, F. Roder, S. Thiede, C. Herrmann, U. Krewer, *J. Electrochem. Soc.* **2020**, *167*, 060501.

[12] A. C. Ngandjong, T. Lombardo, E. N. Primo, M. Chouchane, A. Shodiev, O. Arcelus, A. A. Franco, *J. Power Sources* **2021**, *485*, 229320.

[13] M. Thomitzek, O. Schmidt, G. Ventura Silva, H. Karaki, M. Lippke, U. Krewer, D. Schroder, A. Kwade, C. Herrmann, *Sustainability* **2022**, *14*, 1530.

[14] D. Solle, B. Hitzmann, C. Herwig, M. Pereira Remelhe, S. Ulonska, L. Wuerth, A. Prata, T. Steckenreiter, *Chem. Ing. Tech.* **2017**, *89*, 542.

[15] F. M. Zanotto, D. Z. Dominguez, E. Ayerbe, I. Boyano, C. Burmeister, M. Duquesnoy, M. Eisentraeger, J. F. Montano, A. Gallo-Bueno, L. Gold, F. Hall, N. Kaden, B. Muerkens, L. Otaegui, Y. Reynier, S. Stier, M. Thomitzek, A. Turetskyy, N. Vallin, J. Wessel, X. Xu, J. Abbasov, A. A. Franco, *Batteries Supercaps* **2022**, *5*, 202200224.

[16] C. Lischka, H. Nirschl, *Energy Technol.* **2022**, In review.

[17] T. Lombardo, A. C. Ngandjong, A. Belhcen, A. A. Franco, *Energy Storage Mater.* **2021**, *43*, 337.

[18] M. Lippke, T. Ohnimus, T. Heckmann, D. Ivanov, P. Scharfer, W. Schabel, C. Schilde, A. Kwade, *Energy Technol.* **2022**, https://doi.org/10.1002/ente.202200724.

[19] C. S. Gimenez, B. Finke, C. Schilde, L. Frobose, A. Kwade, *Powder Technol.* **2019**, *349*, 1.

[20] C. Meyer, H. Bockholt, W. Haselrieder, A. Kwade, *J. Mater. Process. Technol.* **2017**, *249*, 172.

[21] A. C. Ngandjong, A. Rucci, M. Maiza, G. Shukla, J. Vazquez-Arenas, A. A. Franco, *J. Phys. Chem. Lett.* **2017**, *8*, 5966.

[22] M. Schonemann, H. Bockholt, S. Thiede, A. Kwade, C. Herrmann, *Int. J. Adv. Manuf. Technol.* **2019**, *102*, 1373.

[23] A. Lamorgese, R. Mauri, B. Tellini, *J. Energy Storage* **2018**, *20*, 289.

[24] H. Karaki, M. Thomitzek, T. Obermann, C. Herrmann, D. Schoder, **2022**, Submitted for publication.

[25] M. Thomitzek, O. Schmidt, T. Abraham, F. Cerdas, F. Roder, U. Krewer, C. Herrmann, *Procedia CIRP* **2021**, *104*, 1059.

[26] H. Bockholt, W. Haselrieder, A. Kwade, *ECS Trans.* **2013**, *50*, 25.

[27] V. Wenzel, R. S. Moeller, H. Nirschl, *Energy Technol.* **2014**, *2*, 176.

[28] W. Bauer, D. Notzel, V. Wenzel, H. Nirschl, *J. Power Sources* **2015**, *288*, 359.

[29] E. Asylbekov, R. Trunk, M. J. Krause, H. Nirschl, *Energy Technol.* **2021**, *9*, 2000850.

[30] P. A. Cundall, O. D. L. Strack, *Geotechnique* **1979**, *29*, 47.

[31] J. K. Mayer, L. Almar, E. Asylbekov, W. Haselrieder, A. Kwade, A. Weber, H. Nirschl, *Energy Technol.* **2020**, *8*, 1900161.

[32] H. Bockholt, M. Indrikova, A. Netz, F. Golks, A. Kwade, *J. Power Sources* **2016**, *325*, 140.

[33] M. Haarmann, W. Haselrieder, A. Kwade, *Energy Technol.* **2020**, *8*, 1801169.

[34] S. H. Sung, S. Kim, J. H. Park, J. D. Park, K. H. Ahn, *Materials* **2020**, *13*, 4544.

[35] B. Finke, Dissertation, Technische Universität Braunschweig, Germany **2022**.

[36] J. Raasch, Dissertation, Technische Hochschule Karlsruhe **1961**, pp. 58, OCLC number: 73980112.

[37] M. Schmitt, R. Diehm, P. Scharfer, W. Schabel, *J. Coat. Technol. Res.* **2015**, *12*, 927.

[38] M. Schmitt, M. Baunach, L. Wengeler, K. Peters, P. Junges, P. Scharfer, W. Schabel, *Chem. Eng. Process. Process Intensif.* **2013**, *68*, 32.

[39] R. Diehm, H. Weinmann, J. Kumberg, M. Schmitt, J. Fleischer, P. Scharfer, W. Schabel, *Energy Technol.* **2020**, *8*, 1900137.

[40] R. Diehm, M. Muller, D. Burger, J. Kumberg, S. Spiegel, W. Bauer, P. Scharfer, W. Schabel, *Energy Technol.* **2020**, *8*, 2000259.

[41] R. Diehm, J. Kumberg, *Energy Technol.* **2020**, *8*, 1901251.

[42] S. Spiegel, T. Heckmann, A. Altvater, R. Diehm, P. Scharfer, W. Schabel, *J. Coat. Technol. Res.* **2022**, *19*, 121.

[43] S. F. Kistler, *Liquid Film Coating: Scientific Principles and their Technological Implications*, Springer Netherlands, Dordrecht **2012**, https://doi.org/10.1007/978-94-011-5342-3.

[44] M. S. Carvalho, H. S. Kheshgi, *AIChE J.* **2000**, *46*, 1907.

[45] J. Nam, M. S. Carvalho, *Chem. Eng. Process. Process Intensif.* **2011**, *50*, 471.

[46] K. J. Ruschak, *Chem. Eng. Sci.* **1976**, *31*, 1057.

[47] B. G. Higgins, L. E. Scriven, *Chem. Eng. Sci.* **1980**, *35*, 673.

[48] S. Jaiser, M. Muller, M. Baunach, W. Bauer, P. Scharfer, W. Schabel, *J. Power Sources* **2016**, *318*, 210.

[49] S. Jaiser, J. Kumberg, J. Klaver, J. L. Urai, W. Schabel, J. Schmatz, P. Scharfer, *J. Power Sources* **2017**, *345*, 97.

[50] J. Kumberg, M. Muller, R. Diehm, S. Spiegel, C. Wachsmann, W. Bauer, P. Scharfer, W. Schabel, *Energy Technol.* **2019**, *7*, 1900722.

[51] J. C. Eser, B. Deichmann, T. Wirsching, L. Merklein, M. Muller, P. Scharfer, W. Schabel, *Drying Technol.* **2020**, *40*, 1130.

[52] J. Kumberg, M. Baunach, J. C. Eser, A. Altvater, P. Scharfer, W. Schabel, *Energy Technol.* **2021**, *9*, 2000889.

[53] J. Kumberg, M. Baunach, J. C. Eser, A. Altvater, P. Scharfer, W. Schabel, *Energy Technol.* **2021**, *9*, 2100013.

[54] P. A. Cundall, O. D. L. Strack, *Geotechnique* **1980**, *30*, 331.

[55] J. K. Mayer, H. Bockholt, A. Kwade, *J. Power Sources* **2022**, *529*, 231259.

[56] M. Zhu, J. Park, A. M. Sastry, *J. Electrochem. Soc.* **2011**, *158*, A1155.

[57] M. Kroupa, M. Vonka, M. Soos, J. Kosek, *Langmuir* **2016**, *32*, 8451.

[58] T. Breinlinger, T. Kraft, *Powder Technol.* **2014**, *256*, 279284.

[59] M. Stein, A. Mistry, P. P. Mukherjee, *J. Electrochem. Soc.* **2017**, *164*, A1616.

[60] C. S. Gimenez, C. Schilde, L. Frobuse, S. Ivanov, A. Kwade, *Energy Technol.* **2020**, *8*, 1900180.

[61] M. Stich, N. Pandey, A. Bund, *J. Power Sources* **2017**, *364*, 84.

[62] F. Huttner, A. Diener, T. Heckmann, J. C. Eser, T. Abali, J. K. Mayer, P. Scharfer, W. Schabel, A. Kwade, *J. Electrochem. Soc.* **2021**, *168*, 090539.

[63] F. Huttner, W. Haselrieder, A. Kwade, *Energy Technol.* **2020**, *8*, 1900245.

[64] F. Huttner, A. Marth, J. C. Eser, T. Heckmann, J. Mohacsi, J. K. Mayer, P. Scharfer, W. Schabel, A. Kwade, *Batteries Supercaps* **2021**, *4*, 1499.

[65] J. C. Eser, B. Deichmann, T. Wirsching, P. G. Weidler, P. Scharfer, W. Schabel, *Langmuir* **2020**, *36*, 6193.

[66] J. C. Eser, T. Wirsching, P. G. Weidler, A. Altvater, T. Buornhorst, J. Kumberg, G. Schuone, M. Muuller, P. Scharfer, W. Schabel, *Energy Technol.* **2020**, *8*, 1801162.

[67] D. Mayer, J. Fleischer, *Procedia CIRP* **2021**, *104*, 744.

[68] F. J. Gunter, J. Keilhofer, C. Rauch, S. Rossler, M. Schulz, W. Braunwarth, R. Gilles, R. Daub, G. Reinhart, *J. Power Sources* **2022**, *517*, 230668.

[69] F. J. Gunter, S. Rossler, M. Schulz, W. Braunwarth, R. Gilles, G. Reinhart, *Energy Technol.* **2020**, *8*, 1801108.

[70] D. L. Wood, J. Li, C. Daniel, *J. Power Sources* **2015**, *275*, 234.

[71] A. Borshchev, A. Filippov, in *The 22nd Inter. Conf. of the System Dynamics Society*, Oxford, England **2004**.

[72] G. V. Silva, M. Thomitzek, T. Abraham, C. Herrmann, *Procedia CIRP* **2021**, *104*, 1017.

[73] V. Laue, F. Roder, U. Krewer, *Electrochim. Acta* **2019**, *314*, 20.

[74] V. Laue, N. Wolff, F. Roder, U. Krewer, *Energy Technol.* **2020**, *8*, 1801049.

[75] D. A. G. Bruggeman, *Ann. Phys.* **1935**, *416*, 636.

[76] T. Gunther, N. Billot, J. Schuster, J. Schnell, F. B. Spingler, H. A. Gasteiger, *Adv. Mater. Res.* **2016**, *1140*, 304.

[77] J. Schunemann, H. Dreger, H. Bockholt, A. Kwade, *ECS Trans.* **2016**, *73*, 153.

[78] A. Diener, S. Ivanov, W. Haselrieder, A. Kwade, *Energy Technol.* **2022**, *10*, 2101033.

[79] S. Thiede, A. Turetskyy, T. Loellhoeffel, A. Kwade, S. Kara, C. Herrmann, *CIRP Ann.* **2020**, *69*, 21.